Intraphase Microstructure–Understanding the Impact on Organic Solar Cell Performance

Fiona H. Scholes, Tino Ehlig, Michael James, Kwan H. Lee, Noel Duffy, Andrew D. Scully, T. Birenda Singh, Kevin N. Winzenberg, Pete Kemppinen, and Scott E. Watkins**

A comprehensive study of the effect of intraphase microstructure on organic photovoltaic (OPV) device performance is undertaken. Utilizing a bilayer device architecture, a small molecule donor (TIPS-DBC) is deposited by both spin-coating and by thermal evaporation in vacuum. The devices are then completed by thermal evaporation of C_{60}, an exciton blocking layer and the cathode. This bilayer approach enables a direct comparison of device performance for donor layers in which the same material exhibits subtle differences in microstructure. The electrical performance is shown to differ considerably for the two devices. The bulk and interfacial properties of the donor layers are compared by examination with photoelectron spectroscopy in air (PESA), optical absorption spectroscopy, charge extraction of photo-generated charge carriers by linearly increasing voltage (photo-CELIV), time-resolved photoluminescence measurements, X-ray reflectometry (XR), and analysis of dark current behavior. The observed differences in device performance are shown to be influenced by changes to energy levels and charge transport properties resulting from differences in the microstructure of the donor layers. Importantly, this work demonstrates that in addition to the donor/acceptor microstructure, the intraphase microstructure can influence critical parameters and can therefore have a significant impact on OPV performance.

1. Introduction

Low cost solar technologies are crucial to achieving the goal of meeting growing global energy demands in a sustainable and greenhouse-friendly manner. While solar cells based on inorganic semiconductors are well known, the past decade has seen substantial advances in thin-film solar cell technologies based on organic semiconductors. These organic photovoltaics (OPVs) are an exciting prospect for harvesting solar energy due to their many beneficial features, such as mechanical flexibility, extremely light weight, and compatibility with low cost manufacturing routes such as printing. Their practical application is still hindered, however, by technical challenges associated with reproducibility, durability and, in particular, efficiency.

Typically, the best power conversion efficiencies for OPVs are achieved using a bulk heterojunction (BHJ) device architecture. This approach creates an extended interface between the electron donor and acceptor materials, together with continuous pathways to the electrodes, thereby maximizing the generation of free charge carriers and optimizing the efficiency of their collection.[1] To date, BHJ devices with power conversion efficiencies of up to 10% have been reported.[2] To improve upon this, a detailed understanding of how material properties and fabrication processes contribute to the performance of OPVs is essential.

BHJ microstructure (morphology) is well known to be a key factor in device performance, since the segregation of donor and acceptor phases on a submicrometer scale has been shown in many studies to have a large effect on efficiency.[3] The screening of candidate materials for more efficient OPVs is made difficult by the complex dependence of BHJ microstructure on preparation conditions. Planar heterojunction (bilayer) OPVs present an alternative device architecture, in which the three-dimensional phase morphology of the donor/acceptor blend is no longer relevant. In principle, bilayer devices possess a single, well-defined planar interface between donor and acceptor, and a direct pathway for charge carriers to the electrodes through

Dr. F. H. Scholes, T. Ehlig, N. Duffy, A. D. Scully,
T. B. Singh, K. N. Winzenberg, P. Kemppinen, Dr. S. E. Watkins
CSIRO Materials Science and Engineering
Private Bag 33, Clayton South MSC,MDC, Victoria 3169, Australia
E-mail: fiona.scholes@csiro.au; scott.watkins@csiro.au
Prof. M. James
Bragg Institute
Australian Nuclear Science and Technology Organisation
Menai, NSW 2234, Australia

Prof. M. James, Dr. K. H. Lee
School of Chemistry
University of New South Wales
Sydney, NSW 2052, Australia
Dr. K. H. Lee
Centre for Organic Photonics and Electronics
School of Molecular Biosciences
The University of Queensland
Brisbane, Queensland 4072, Australia

DOI: 10.1002/adfm.201300726

both materials, making their performance less susceptible to fabrication parameters. While bilayer OPVs generally exhibit lower power conversion efficiencies than their BHJ counterparts due to reduced donor/acceptor interfacial area, they have provided significant insights into OPV performance. Recently, bilayers have been used to evaluate new donor[4] and acceptor compounds.[5] Systematic annealing of bilayers has also been used to study the effect of interfacial roughness[6] and interdiffusion of donor and acceptor components[7,8] on device performance. Microscopic modelling of bilayer OPVs in comparison with BHJs has resulted in an improved understanding of the impact of charge carrier separation and recombination on device performance.[9] Furthermore, enhanced bilayer devices, featuring a combination of doped and additional layers, have been shown to give some of the highest efficiency devices reported.[10,11]

Experimentally, bilayer OPVs offer the opportunity to study changes in the donor or acceptor layer, while the preparation of all other layers in the device remains unchanged. In this paper, we report on a comparative study of bilayer OPVs in which the same donor material is deposited using two different methods. In general, OPVs fall into two distinct classes: i) those in which the active layer is deposited from solution, and ii) those in which the active layer is deposited via thermal evaporation in vacuum. Solution-processable materials have the greatest commercial potential in low-cost printing technologies, whereas evaporative processing offers more controlled deposition. A comparison of solution-processed and vacuum-deposited OPVs was recently reported by Kronenberg et al.,[12] in which they found that their OPVs performed better when prepared by vacuum methods. However, their study involved a BHJ device architecture, and while the merocyanine donor materials could be processed by both solution and vacuum methods, a different acceptor material was used for the solution-processed and vacuum-deposited cells (the soluble fullerene derivative $PC_{60}BM$, and C_{60}, respectively).

Here, we utilize the bilayer OPV device architecture to make a direct comparison of a solution-processed and vacuum-deposited donor while the preparation of all other layers, including the acceptor layer, remains unchanged. The compound 7,14-bis((triisopropylsilyl)-ethynyl)dibenzo[*b,def*]chrysene (TIPS-DBC, **Figure 1**a) is used as the donor material. The dibenzo[*b,def*]chrysene template has been shown to be a promising candidate for use in organic electronic devices, due to its straightforward and reproducible synthesis from inexpensive starting materials, the ease with which it can be purified, its stability under ambient laboratory conditions, and measured power conversion efficiency of 2.22% in BHJ devices with $PC_{60}BM$.[13] Importantly, TIPS-DBC can be processed both from solution and by thermal evaporation in vacuum, making it ideal for studying the differences between bilayer OPVs fabricated using these two different methods. In this study, the bilayer device is completed by subsequent vacuum deposition of a C_{60} acceptor layer, avoiding potential dissolution effects at the donor/acceptor interface by a solution-processed acceptor layer. Using this approach, we demonstrate that it is possible to probe the differences in bulk and interfacial properties of the TIPS-DBC layer prepared by the two different methods, and to relate these differences to device performance. More generally, this study highlights how subtle differences in intraphase microstructure can have a significant impact on OPV performance.

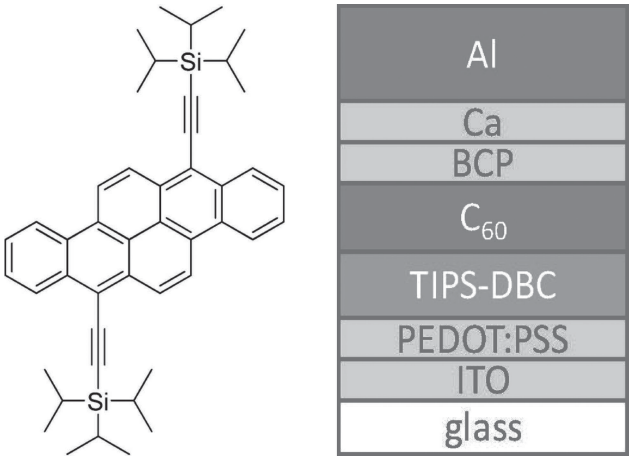

Figure 1. a) Molecular structure of the donor compound (TIPS-DBC), and b) schematic of the bilayer solar cells. The donor layer is either spin-coated from solution or deposited by thermal evaporation in vacuum.

2. Results and Discussion

The dependence of device performance on TIPS-DBC and C_{60} layer thicknesses was investigated first, using vacuum deposition for both materials. A total of 16 devices, each with a different TIPS-DBC/C_{60} layer thickness combination, were prepared simultaneously in order to eliminate batch-to-batch variation. The results are shown in **Figure 2** and demonstrate that optimum power conversion efficiency was reached with 30 nm TIPS-DBC and 35–40 nm C_{60}. The open-circuit voltage (V_{oc}), short-circuit current density (J_{sc}) and fill factor (FF) were found to reach their maximum values at similar layer thicknesses. Thus, in subsequent experiments these optimum layer thicknesses were used for both evaporated and solution-processed devices.

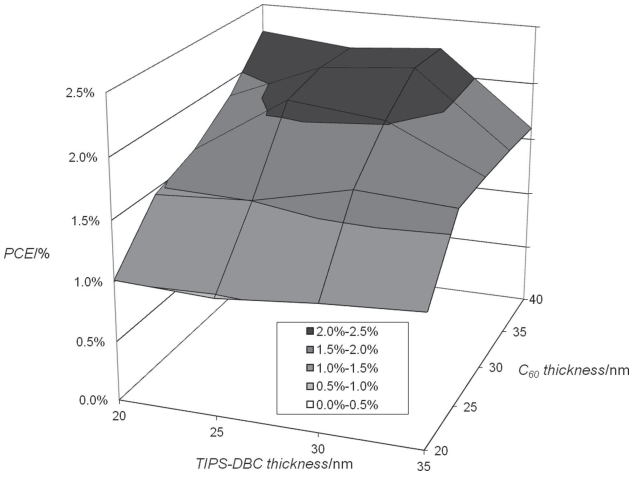

Figure 2. Device efficiency as a function of TIPS-DBC (evaporated) and C_{60} layer thicknesses.

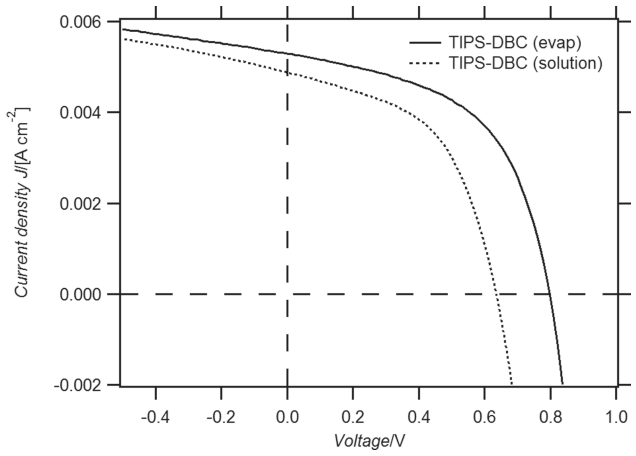

Figure 3. AM1.5 photovoltaic characteristics of TIPS-DBC (30 nm)/C_{60} (40 nm) bilayer devices in which TIPS-DBC is deposition by evaporation (solid curve) or spin-coating (dashed curve). The corresponding solar cell parameters are summarized in Table 1.

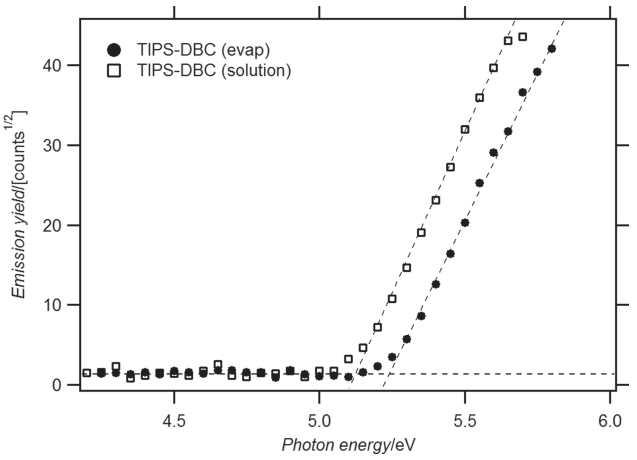

Figure 4. Representative photoelectron spectroscopy in air (PESA) measurements of TIPS-DBC (30 nm) films on PEDOT:PSS/glass substrates.

The trends observed also provide insight into the mechanisms underlying the performance of these devices. The efficiency is almost constant with TIPS-DBC thickness up to 30 nm, but drops sharply at 35 nm, particularly for C_{60} thicknesses of 30 nm or more. Furthermore, efficiency is seen to improve with increasing C_{60} thickness and plateau at a maximum at 35–40 nm. Together, these trends suggest that device performance is limited by hole mobility, with the optimum film thicknesses achieving a balance between hole transport in TIPS-DBC and the higher electron mobility in C_{60}. Previous studies of the effect of film thicknesses on charge imbalance in bilayer OPVs have shown similar findings, with optical absorption and exciton diffusion length also playing a role.[14,15] Furthermore, these results are consistent with previously reported field-effect transistor (FET) measurements, which gave a hole mobility of $\approx 10^{-5}$ to 10^{-3} cm^2 V^{-1} s^{-1} for TIPS-DBC[16] and up to 6 cm^2 V^{-1} s^{-1} for C_{60}.[17]

Figure 3 compares the performance measured for our highest efficiency devices in which the TIPS-DBC layer was deposited from solution and by thermal evaporation in vacuum. The electrical characteristics of the devices are clearly different (see summary in **Table 1**), with the evaporated TIPS-DBC device showing higher V_{oc}, J_{sc}, *FF* and power conversion efficiency (η). Most notably, in the evaporated device the V_{oc} exceeds that of the spin-coated device by 160 mV. This represents a significant difference and demonstrates that although bilayer OPVs are simpler to prepare and optimise than their BHJ counterparts, their performance still depends critically on preparation conditions.

In order to better understand the observed differences in device performance, bulk and interfacial properties of the evaporated and spin-coated TIPS-DBC films were investigated. **Figure 4** shows the results of photoelectron spectroscopy in air (PESA) measurements on TIPS-DBC films prepared on PEDOT:PSS/glass substrates using the same preparation conditions and film parameters as those used for the corresponding OPV devices. The ionization potential determined by PESA is clearly different for the two different films, with values of 5.21 ± 0.01 eV and 5.13 ± 0.01 eV obtained for the evaporated and spin-coated films, respectively. Notably, the results obtained were highly reproducible, with quoted uncertainties resulting from independent measurements of 4 evaporated films and 9 spin-coated films. Since the ionization potential relates to the position of the highest occupied molecular orbital (HOMO), the values obtained here indicate that the HOMO is 0.08 ± 0.02 eV deeper in the evaporated film. Thus, the position of the energy levels in the TIPS-DBC donor layer appears to be modified by the method of preparation.

For BHJ OPVs, it is generally proposed that V_{oc} is related to the energy difference between the HOMO of the donor and the lowest unoccupied molecular orbital (LUMO) of the acceptor.[18] In the case of the bilayer OPVs prepared in this study, the position of the LUMO in the C_{60} acceptor layer should be the same for all devices because all C_{60} layers were prepared under identical conditions. Hence, in the absence of other influences, the difference observed in the HOMO position of the TIPS-DBC donor layer should correlate with the difference observed in V_{oc}. While the V_{oc} measured for the evaporated device was indeed larger, therefore correlating with the deeper HOMO measured by PESA, the measured differences in V_{oc}

Table 1. Solar cell parameters for optimized thickness bilayer devices.

	TIPS-DBC deposition method			
	evaporated (best)[a)]	spin-coated (best)[a)]	evaporated (average)[b)]	spin-coated (average)[b)]
V_{oc} [V]	0.80	0.64	0.79 ± 0.00	0.61 ± 0.04
J_{sc} [mA cm^{-2}]	5.29	4.88	5.12 ± 0.19	4.76 ± 0.21
FF	0.53	0.51	0.52 ± 0.01	0.50 ± 0.03
efficiency, η [%]	2.24	1.58	2.10 ± 0.10	1.45 ± 0.08

[a)]Best devices correspond to those with highest efficiency; [b)]Average (± standard deviation) calculated from 6 devices.

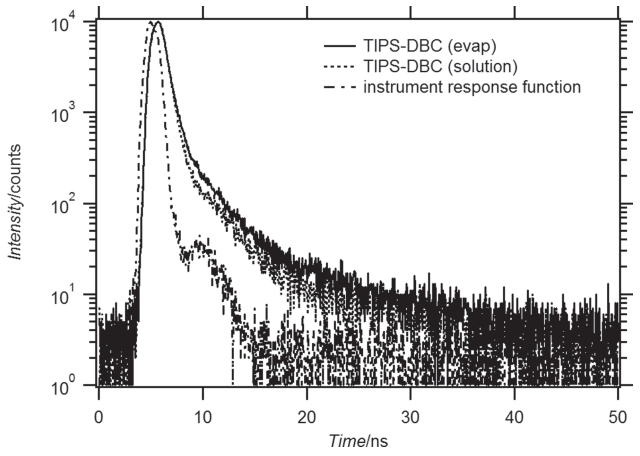

Figure 5. Time-resolved photoluminescence spectra from evaporated (solid) and spin-coated (dashed) TIPS-DBC films.

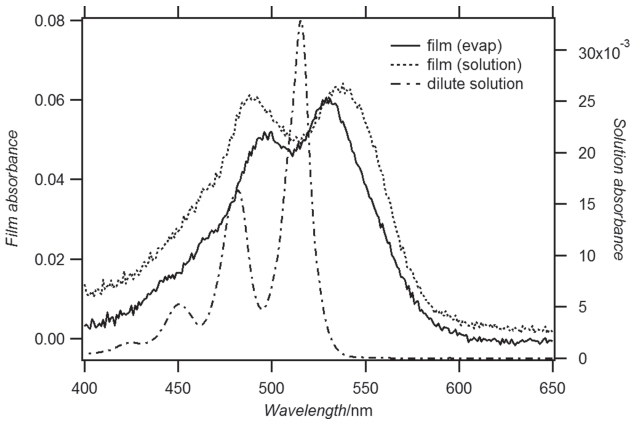

Figure 6. Optical absorption spectra of TIPS-DBC films prepared by evaporation (solid curve) and spin-coating (dashed curve) onto PEDOT:PSS/glass substrates, together with spectrum from dilute solution of TIPS-DBC in toluene (dot-dash curve).

(160 mV) and work function (80 meV) are not the same. This discrepancy suggests that factors other than the position of the energy levels contribute to the differences observed in device performance.

In order to investigate these differences further, TIPS-DBC films were examined using charge extraction of photogenerated charge carriers by linearly increasing voltage (photo-CELIV). Bulk hole mobilities of 4.0 (±1.0) × 10^{-4} and 1.2 (±1.0) × 10^{-3} cm^2 V^{-1} s^{-1} were obtained for evaporated and spin-coated TIPS-DBC films, respectively. While experimental uncertainties are large, it does appear that the mobility for the spin-coated film is generally higher. This suggests that molecular packing in spin-coated TIPS-DBC may be different and, as a consequence, more efficient for hole transport.[19] These bulk mobilities are somewhat different from the FET mobilities reported previously,[16] although it is likely that the latter are much more sensitive to interfacial parameters.

The TIPS-DBC films were also examined by time-resolved PL measurements. A weak, unstructured photoluminescence band centred at ≈600 nm is observed for both films, which is considerably red-shifted compared with the structured fluorescence from a dilute solution of TIPS-DBC in toluene (λ_{max} = 521 nm). Time-resolved PL measurements revealed that the singlet exciton lifetime for the evaporated TIPS-DBC film is marginally longer than that for the spin-coated film (see **Figure 5**). This implies that the mean exciton diffusion length is longer in the evaporated TIPS-DBC layer, and therefore that the yield of excitons reaching the TIPS-DBC/C_{60} heterojunction is higher. This may be a small but contributing factor to the higher efficiency measured for the evaporated TIPS-DBC devices.

The optical absorption spectra of TIPS-DBC films prepared by spin-coating and by thermal evaporation in vacuum are shown in **Figure 6**, together with the absorption spectrum of a dilute solution of TIPS-DBC in toluene. The pronounced red-shift in the absorption spectra of both films compared with that of unassociated molecules in dilute solution is indicative of J· aggregate formation in the solid state.[20] Interestingly, the red-shift for the spin-coated film is larger than that for the evaporated film, demonstrating a clear difference in the bulk optical properties of the two films. Since absorption spectra are sensitive to the nature and extent of molecular aggregation, the observed spectral differences suggest that TIPS-DBC adopts a different microstructure when evaporated compared with when deposited from solution. This also correlates with previously reported atomic force microscopy (AFM) results, in which the topography of spin-coated and evaporated TIPS-DBC films was shown to differ.[16]

Furthermore, differences can also be seen in the incident-photon-to-converted-electron (IPCE) spectral profiles from the corresponding TIPS-DBC/C_{60} devices (**Figure 7**), with the spectrum for the spin-coated TIPS-DBC film exhibiting a 15 nm red-shift in the main peak and an overall lower generation yield. These IPCE results indicate more efficient charge carrier generation and/or reduced recombination in devices with evaporated TIPS-DBC, and are consistent with the higher J_{sc} and η observed from these devices (Table 1). These differences likely arise from differences in the microstructure of the two different TIPS-DBC films.

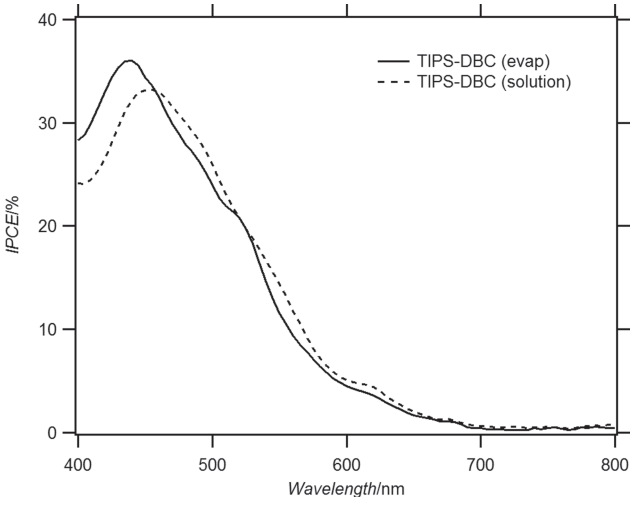

Figure 7. IPCE spectra of devices with evaporated and spin-coated TIPS-DBC films.

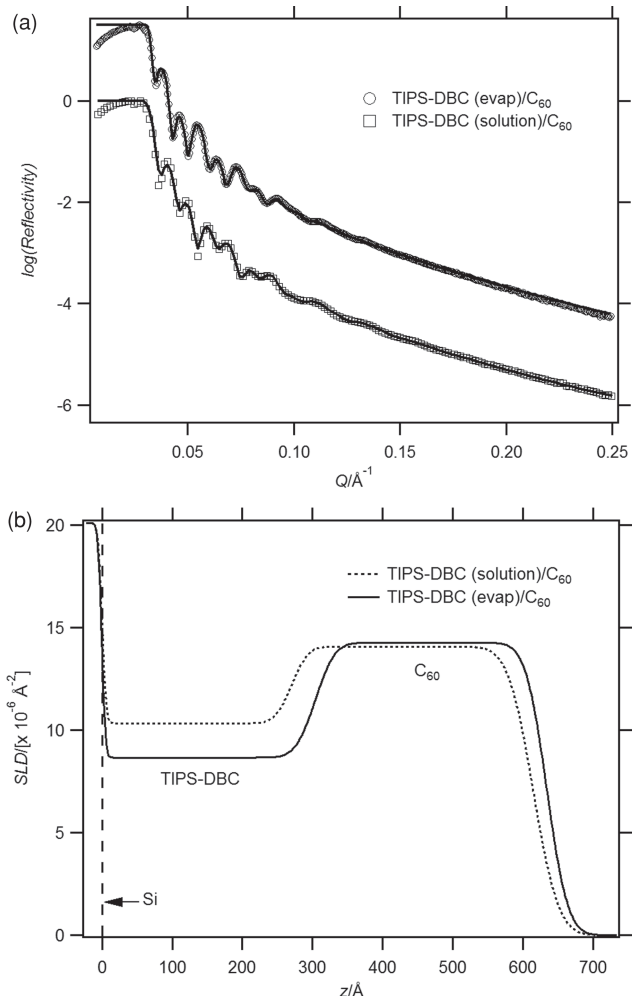

Figure 8. X-ray reflectivity (XR) profiles (top) and calculated models (bottom) of TIPS-DBC/C_{60} bilayer films on Si wafers, for both evaporated and spin-coated TIPS-DBC. XR profiles have been offset for clarity. Film thickness (z) is referenced to Si at the origin.

To further investigate the microstructure of TIPS-DBC/C_{60} OPVs, the corresponding bilayers were studied by X-ray reflectometry (XR). **Figure 8** shows the measured data together with their fits, as well as the SLD profiles (i.e., representing vertical composition) obtained from fitting the XR data. The resulting fitting parameters are summarized in **Table 2**. Both evaporated and spin-coated TIPS-DBC/C_{60} bilayers fitted well to a two-layer model. The calculated SLD for C_{60} is as expected based on its known bulk mass density.[21] The expected SLD for TIPS-DBC based on its bulk mass density determined from single crystal X-ray diffraction[16] is 10.5×10^{-6} Å^{-2}. Interestingly, the SLD for the spin-coated TIPS-DBC layer (10.3×10^{-6} Å^{-2}) is 18% larger than that for the evaporated film (8.7×10^{-6} Å^{-2}), with the corresponding values also obtained in the absence of C_{60} (not shown) and the former being comparable to that expected from the bulk crystalline state. These results confirm that there is little, if any, interdiffusion between layers and therefore that the bilayer architecture is maintained after preparation. Moreover,

Table 2. Calculated fitting parameters from X-ray reflectivity profiles of TIPS-DBC/C_{60} bilayers on Si. Numbers in parenthesis represent interfacial roughness (in Å).

	TIPS-DBC deposition method			
	Evaporated[a)]		spin-coated[b)]	
	SLD [×10^{-6}Å^{-2}]	thickness [Å]	SLD [×10^{-6}Å^{-2}]	thickness [Å]
C_{60}	14.3	330 (24)	14.1	327 (27)
TIPS-DBC	8.7	304 (22)	10.3	257 (18)
Si	20.1	inf (4)	20.1	inf (4)

[a)]Fit statistics: $\chi^2 = 0.004$; [b)]Fit statistics: $\chi^2 = 0.002$.

the results indicate that the film is more densely packed when deposited by spin-coating, and confirm that there is indeed a microstructural difference between the TIPS-DBC layers deposited by the two different methods.

To gain further insight into charge transport properties in these devices, the dependence of J_{sc} on light intensity, I, was investigated and the results are shown in **Figure 9**. It has been shown that the photocurrent is proportional to I^{α} where the exponent $\alpha = 1$ in the space-charge-free limit.[22] Here, it can be seen that J_{sc} is directly proportional to light intensity, i.e., $\alpha = 1$, for devices prepared with either evaporated or spin-coated TIPS-DBC. This result indicates that, at short circuit conditions, the build-up of space charge in these devices is negligible, and shows that geminate recombination is the dominant recombination mechanism as expected for bilayer devices.[9,23] Evidently, these factors do not contribute to the difference observed in the efficiency of devices prepared with evaporated and spin-coated TIPS-DBC.

In order to explore the relationship between intermolecular interactions and performance, dark currents from the devices were measured and analyzed in the manner described by Perez et al.[24] The results are shown in **Figure 10** and **Table 3**. The calculated values of V_{oc} are in good agreement with the measured

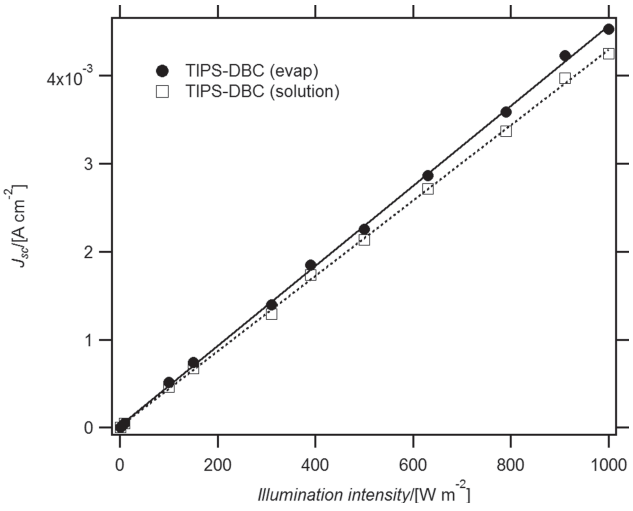

Figure 9. The short-circuit current density, J_{sc}, as a function of illumination intensity, together with linear fits to the data (lines).

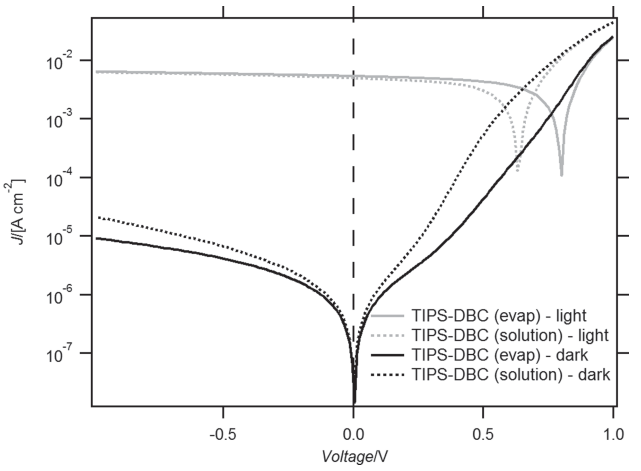

Figure 10. Current density versus voltage characteristics in the dark (black) and under illumination (grey).

values, indicating that the model used to fit the data is valid. While evaporated and spin-coated TIPS-DBC have very similar values of ΔE_{DA} (the interfacial energy gap corresponding to the difference in energy between the HOMO of the donor and the LUMO of the acceptor) as estimated from PESA measurements (see Figure 4), the calculations show that their J_{S0} (saturation dark current term) values differ by about an order of magnitude. This explains why the discrepancy in V_{oc} is larger than that predicted by ΔE_{DA} alone (see Equation 2). Moreover, this can be attributed to differences in intermolecular coupling at the donor/acceptor interface.[24,25]

In previous work, Perez et al. compared J_{S0} for tetracene and rubrene in planar heterojunction devices with C_{60}, and found a much larger value of J_{S0} for tetracene which they attributed to stronger tetracene/tetracene and tetracene/C_{60} coupling. This could be explained by the planar geometry of tetracene, which results in stronger intermolecular interactions compared with the sterically-hindered, non-planar rubrene molecule. The weaker interactions for rubrene result in kinetic suppression of dark recombination and therefore an unexpectedly large photovoltage.[24]

In this study, Table 3 shows that J_{S0} is larger for devices prepared with spin-coated TIPS-DBC. This suggests that solution processing results in a thin film microstructure in which there are stronger intermolecular interactions between TIPS-DBC molecules as well as between TIPS-DBC and C_{60} at the heterojunction. This, in turn, contributes to enhanced recombination and therefore a lower V_{oc}. This conclusion is consistent with the IPCE spectral measurements (Figure 7), which indicated enhanced recombination in devices with spin-coated TIPS-DBC. It is also in agreement with XR measurements which gave a higher SLD for spin-coated TIPS-DBC (see Table 2) suggesting a more densely packed film. Finally, it also correlates with the results of photo-CELIV, time-resolved photoluminescence (Figure 5) and optical absorption spectroscopy (Figure 6) which all exhibited differences between spin-coated and evaporated films attributable to differences in TIPS-DBC microstructure. Clearly, the microstructure of the donor phase itself (i.e., in addition to the more commonly considered microstructure relating to donor-acceptor phase segregation in BHJ devices) can be controlled by the method by which the thin film is prepared, affecting a range of properties that can have a substantial impact on OPV performance.

Table 3. Comparison of measured and calculated parameters based on dark and light performance measurements (ΔE_{DA} in eV, J_{S0} in A cm^{-2}, V_{oc} in V).

	TIPS-DBC deposition method	
	evaporated	spin-coated
ΔE_{DA}	1.71	1.63
J_{S0} - calculated	0.34×10^{-2}	4.7×10^{-2}
V_{oc} - calculated	0.89	0.70
V_{oc} - measured	0.80	0.64

3. Conclusions

A comprehensive comparison has been presented of bilayer OPV devices in which the donor layer, TIPS-DBC, was prepared by two different methods. The electrical performance of the corresponding TIPS-DBC/C_{60} devices was found to differ considerably, with evaporated TIPS-DBC giving higher V_{oc}, J_{sc}, FF and η than devices prepared with spin-coated TIPS-DBC. We have examined these devices, together with the bulk and interfacial properties of the TIPS-DBC layers, and have provided evidence for the dependence of performance on the microstructure of the TIPS-DBC film. Specifically, we have shown that spin-coated TIPS-DBC produces a more densely packed film than that prepared by evaporation. This, in turn, has been shown to influence the position of the TIPS-DBC HOMO, the recombination rate and, to a lesser extent, the exciton diffusion length. Devices made with an evaporated donor layer, which results in reduced intermolecular associations, perform better. This study highlights the importance of the microstructure within the donor layer itself, that is, not just the microstructure relating to donor/acceptor phase segregation in BHJ devices. It also suggests that, for some materials, it is possible to tune the microstructure of the donor layer in bilayer OPVs to achieve a high ΔE_{DA} and low J_{S0} in order to produce an optimized device with high open circuit voltage. This study also illustrates that the simplified architecture of bilayer OPVs can provide significant insights into the various materials properties that can influence OPV performance.

4. Experimental Section

Device Preparation: ITO-coated glass substrates (Lumtec, 5 Ω sq^{-1}) were cleaned by successively sonicating in acetone and iso-propanol (each 10 min). The substrates were then exposed to a UV-ozone clean (Novascan PDS-UVT, 10 min). PEDOT/PSS (HC Starck, Baytron P AI 4083) was filtered (0.2 μm RC filter) and deposited by spin-coating (5000 rpm, 20 s). The PEDOT/PSS layer was then annealed on a hotplate in a N_2 glovebox (150 °C, 5 min).

TIPS-DBC was synthesized as previously reported.[13] For devices with spin-coated TIPS-DBC layers, TIPS-DBC (3.0 mg mL^{-1}) was dissolved in chloroform (Aldrich, anhydrous) and deposited onto PEDOT:PSS-coated substrates inside a glovebox by static spin-coating (5000 rpm,

30 s). The concentration and spin speed were optimised to match the film thickness of the best-performing evaporated TIPS-DBC device. These devices were then transferred (without exposure to air) to a vacuum evaporator (Angstrom Engineering Inc.) equipped with a variety of masks and a gradient shutter. For devices with evaporated TIPS-DBC layers, PEDOT:PSS-coated substrates were transferred (without exposure to air) to the same vacuum evaporator and TIPS-DBC was deposited by thermal evaporation from an alumina crucible (at a rate of 0.5 Å s^{-1}). Film thicknesses for both spin-coated and evaporated films were determined using an atomic force microscope.

Following deposition of TIPS-DBC, all subsequent layers were deposited without breaking vacuum at pressures below 2×10^{-6} mbar. C_{60} (Nano-C) was deposited by thermal evaporation from an alumina crucible (at a rate of 0.5 Å s^{-1}) and with layer thicknesses as described. Bathocuproine (BCP, Sigma-Aldrich) was then deposited from an alumina crucible (10 nm, 0.5 Å s^{-1}) as an exciton blocking layer. Lastly, a layer of Ca (Sigma-Aldrich, 20 nm, 0.5 Å s^{-1}) and Al (Kurt J. Lesker, 100 nm, 1 Å s^{-1}) were deposited through a shadow mask to make the cathode. The area defined by the shadow mask gave device areas of 0.2 cm^2. A device schematic is shown in Figure 1b.

The completed devices were then encapsulated with glass and a UV-cured epoxy (Summers Optical, Lens Bond type J-91) by exposing to 365 nm UV light inside a N_2 glovebox (10 min). The encapsulated devices were then removed from the glovebox and tested in air within 1 h.

Current-Voltage (J-V) Characteristics: The cells were tested with an Oriel solar simulator fitted with a 1000 W Xe lamp filtered to give an output of 100 mW cm^{-2} at AM1.5. The lamp was calibrated using a standard, filtered Si cell from Peccell Limited which was subsequently cross-calibrated with a standard reference cell traceable to the National Renewable Energy Laboratory. The devices were tested using a Keithley 2400 Sourcemeter controlled by Labview software. The *J-V* characteristics of the solar cells were measured and device performance extracted from the *J-V* data. For light intensity dependence measurements, *J-V* curves were acquired as described but with a series of neutral density filters in front of the devices ranging from 0.1% to 100% transmission.

IPCE Measurements: IPCE ratio data was collected using an Oriel 150 W Xe lamp coupled to a monochromator and an optical fibre. The output of the optical fiber was focussed to give a beam that was contained within the area of the device. IPCE data was calibrated with a standard, unfiltered Si cell.

Dark Current Measurements and Analysis: Dark currents from the devices were measured and analyzed in the manner described by Perez et al.[24] *J-V* characteristics were collected as described above, but without illumination. The dark current *J-V* characteristics were then fitted to a simplified Shockley equation (see Equation 2 in Perez et al.[24]) to extract values for the diode ideality factor (n) and the saturation current density (J_S). The pre-exponential saturation dark current term (J_{S0}) was then calculated according to:[24]

$$J_S = J_{S0} \exp\left(-\frac{\Delta E_{DA}}{2nkT}\right) \quad (1)$$

Here, the position of the HOMO for TIPS-DBC was taken from the results of PESA (see below), and the LUMO for C_{60} (3.5 eV) was obtained from the literature.[26] V_{oc} was then calculated using J_{S0}, ΔE_{DA} and the measured value for J_{sc} as previously described[24] using the following equation:

$$V_{oc} = \frac{nkT}{q} ln\left(\frac{J_{sc}}{J_{S0}}\right) + \frac{\Delta E_{DA}}{2q} \quad (2)$$

where q is the fundamental charge and the temperature $T = 298$ K.

Photoelectron Spectroscopy in Air: Photoelectron spectroscopy in air (PESA) measurements were recorded with a Riken Keiki AC-2 PESA spectrometer with a power setting of 5 nW and a power number of 0.5. Samples for analysis were prepared by either spin-coating or thermal evaporation of TIPS-DBC onto glass substrates, using the deposition conditions above.

Photophysical Measurements: Optical absorption spectra of solutions and unencapsulated films were recorded using a Hewlett Packard HP 8453 Diode Array UV-visible spectrophotometer. Spectra were recorded in transmission mode at normal incidence. Samples for analysis were the same as those prepared for PESA. Time-resolved photoluminescence (PL) from the films was measured at 600 nm using an Edinburgh Instruments Ltd. FLSP920 time-correlated single-photon counting spectrometer comprising a pulsed diode laser excitation source operating at 467 nm.

Charge mobilities were obtained using the photo-CELIV technique (photo-induced charge extraction by linearly increasing voltage) using instrumentation described previously.[27] In brief, the measurements were conducted using glass-encapsulated devices and a pulsed nitrogen laser (Laser Science Inc. VSL-337) with an output at 337 nm (pulse duration ≈4 ns, pulse energy ≈0.1 mJ). The voltage ramp was generated using a function generator (Agilent 33250), and the extraction currents were recorded using a 500 MHz oscilloscope (Tektronix DPO3054) and a variable resistor. The delay in the triggering of the voltage ramp after triggering of the laser pulse was controlled using a delay/pulse generator (Stanford Research Systems DG535).

X-Ray Reflectometry: X-ray reflectivity profiles were measured using a Panalytical Ltd. X'Pert Pro Reflectometer and Cu Kα X-ray radiation (λ = 1.540598 Å). The pre-sample X-ray beam was collimated using a Göbel mirror and a 0.1 mm slit, and the post-sample beam by a parallel plate collimator. Reflectivity data were collected using a NaI scintillation detector over the angular range $0.05° \leq \theta \leq 5.00°$, with a step size of 0.010° and counting times of 10 s per step. The observed X-ray reflectivity profiles are presented as a function of the momentum transfer normal to the sample surface ($Q_z = 4\pi(\sin\theta)/\lambda$). Analysis of the reflectivity profiles was performed using a slab model and the Motofit program.[28] The Levenberg-Marquardt least squares minimisation algorithm was used to extract thickness, scattering length density (SLD, where SLD = $r_e N_A \rho Z/M$ and r_e is the Bohr electron radius, N_A is Avogadro's number, ρ is the mass density, Z is the atomic number and M is the molar mass of the molecular species in the film), and interfacial roughness values for each layer from a structural model based on the fitted reflectivity.

Acknowledgements

This research was funded through the Flexible Electronics Theme of the CSIRO Future Manufacturing Flagship and was also supported by the Victorian Organic Solar Cell Consortium (Victorian Department of Primary Industries, Sustainable Energy Research and Development Grant; Victorian Department of Business and Innovation, Victoria's Science Agenda Grant; and the Australian Solar Institute). X-ray reflectometry measurements were performed at the Bragg Institute and were supported by the Australian Nuclear Science and Technology Organisation and the Australian Institute of Nuclear Science and Engineering.

Received: February 27, 2013
Revised: April 2, 2013
Published online: May 16, 2013

[1] N. S. Sariciftci, L. Smilowitz, A. J. Heeger, F. Wudl, *Science* **1992**, *258*, 1474.
[2] M. A. Green, K. Emery, Y. Hishikawa, W. Warta, E. D. Dunlop, *Prog. Photovolt: Res. Appl.* **2012**, *20*, 12.
[3] F. Liu, Y. Gu, J. W. Jung, W. H. Jo, T. P. Russell, *J. Polym. Sci., Part B: Polym. Phys.* **2012**, *50*, 1018.
[4] A. Yassin, T. Rousseau, P. Leriche, A. Cravino, J. Roncali, *Sol. Energy Mater. Sol. Cells* **2011**, *95*, 462.
[5] J. L. Yang, S. Schumann, R. A. Hatton, T. S. Jones, *Org. Electron.* **2010**, *11*, 1399.

[6] H. P. Yan, S. Swaraj, C. Wang, I. Hwang, N. C. Greenham, C. Groves, H. Ade, C. R. McNeill, *Adv. Funct. Mater.* **2010**, *20*, 4329.
[7] D. Chen, F. Liu, C. Wang, A. Nakahara, T. P. Russell, *Nano Lett.* **2011**, *11*, 2071.
[8] K. H. Lee, P. E. Schwenn, A. R. G. Smith, H. Cavaye, P. E. Shaw, M. James, K. B. Krueger, I. R. Gentle, P. Meredith, P. L. Burn, *Adv. Mater.* **2011**, *23*, 766.
[9] R. A. Marsh, C. Groves, N. C. Greenham, *J. Appl. Phys.* **2007**, *101*, 083509.
[10] R. Fitzner, C. Elschner, M. Weil, C. Uhrich, C. Korner, M. Riede, K. Leo, M. Pfeiffer, E. Reinold, E. Mena-Osteritz, P. Bauerle, *Adv. Mater.* **2012**, *24*, 675.
[11] R. Fitzner, E. Reinold, A. Mishra, E. Mena-Osteritz, H. Ziehlke, C. Korner, K. Leo, M. Riede, M. Weil, O. Tsaryova, A. Weiss, C. Uhrich, M. Pfeiffer, P. Bauerle, *Adv. Funct. Mater.* **2011**, *21*, 897.
[12] N. M. Kronenberg, V. Steinmann, H. Buerckstuemmer, J. Hwang, D. Hertel, F. Wuerthner, K. Meerholz, *Adv. Mater.* **2010**, *22*, 4193.
[13] K. N. Winzenberg, P. Kemppinen, G. Fanchini, M. Bown, G. E. Collis, C. M. Forsyth, K. Hegedus, T. B. Singh, S. E. Watkins, *Chem. Mater.* **2009**, *21*, 5701.
[14] C.-F. Lin, M. Zhang, S.-W. Liu, T.-L. Chiu, J.-H. Lee, *Int. J. Mol. Sci.* **2011**, *12*, 476.
[15] S. Heutz, P. Sullivan, B. M. Sanderson, S. M. Schultes, T. S. Jones, *Sol. Energy Mater. Sol. Cells* **2004**, *83*, 229.
[16] K. B. Burke, Y. Shu, P. Kemppinen, B. Singh, M. Bown, I. I. Liaw, R. M. Williamson, L. Thomsen, P. Dastoor, W. Belcher, C. Forsyth, K. N. Winzenberg, G. E. Collis, *Cryst. Growth Des.* **2012**, *12*, 725.
[17] T. B. Singh, N. S. Sariciftci, H. Yang, L. Yang, B. Plochberger, H. Sitter, *Appl. Phys. Lett.* **2007**, *90*, 213512.
[18] M. C. Scharber, D. Wuhlbacher, M. Koppe, P. Denk, C. Waldauf, A. J. Heeger, C. L. Brabec, *Adv. Mater.* **2006**, *18*, 789.
[19] J. L. Bredas, J. P. Calbert, D. A. da Silva, J. Cornil, *Proc. Natl. Acad. Sci. USA* **2002**, *99*, 5804.
[20] F. Wurthner, T. E. Kaiser, C. R. Saha-Moller, *Angew. Chem. Int. Ed.* **2011**, *50*, 3376.
[21] K. Prassides, H. Kroto, *Phys. World* **1992**, *5*, 44.
[22] V. D. Mihailetchi, J. Wildeman, P. W. M. Blom, *Phys. Rev. Lett.* **2005**, *94*, 126602.
[23] V. D. Mihailetchi, H. X. Xie, B. de Boer, L. J. A. Koster, P. W. M. Blom, *Adv. Funct. Mater.* **2006**, *16*, 699.
[24] M. D. Perez, C. Borek, S. R. Forrest, M. E. Thompson, *J. Am. Chem. Soc.* **2009**, *131*, 9281.
[25] C. W. Schlenker, M. E. Thompson, *Chem. Commun.* **2011**, *47*, 3702.
[26] R. Schwedhelm, L. Kipp, A. Dallmeyer, M. Skibowski, *Phys. Rev. B* **1998**, *58*, 13176.
[27] A. Pivrikas, M. Ullah, T. B. Singh, C. Simbrunner, G. Matt, H. Sitter, N. S. Sariciftci, *Org. Electron.* **2011**, *12*, 161.
[28] A. Nelson, *J. Appl. Crystallogr.* **2006**, *39*, 273.